

## INTEGRATION OF PIV DATA INTO THE SIMPLE ALGORITHM FOR 2D TIME-AVERAGED TURBULENT FLOWS

**Nikolaos-Petros Pallas**

School of Mechanical Engineering  
National Technical University of Athens  
9 Heron Polytechniou, 15773 Zografou, Greece  
Email: npallas@mail.ntua.gr

**Demetri Bouris**

School of Mechanical Engineering  
National Technical University of Athens  
9 Heron Polytechniou, 15773 Zografou, Greece  
Email: dbouris@fluid.mech.ntua.gr

### ABSTRACT

The merging of diverse sources of information describing the same phenomenon is currently an active area of scientific research. In this scope, an attempt based on the SIMPLE algorithm is presented for the integration of time-averaged planar PIV velocity measurements into a CFD code. The measurements are adjusted/corrected by the CFD calculation of the time-averaged velocity fields through which the respective pressure fields are also computed. Boundary conditions are applied based on the PIV data by imposing a layer of constant velocity values near the boundaries i.e. constant first and second normal derivatives. The novelty of this approach derives not only from the integration of PIV measurements but also from the utilisation of PIV statistics for the direct computation of the Reynolds Stresses and their introduction into the source terms of the Reynolds averaged equations. This permits application to steady state turbulent flow fields without the need for a numerical turbulence closure model. The application is the case of a cube with openings, immersed in a boundary-layer flow at an angle of attack equal to 0 degrees. The calculated velocity fields as well as the respective pressure fields are found to be physically consistent, while the inherent turbulent structure of the flow is taken into account.

### INTRODUCTION

The traditional approach in the field of Fluid Mechanics treats the solutions acquired through CFD and Experimental Fluid Mechanics as discrete and separate sources of information, even though they may refer to a common phenomenon. For that reason, the integration of measurements into a CFD code is a significant advancement, in order to capitalise on both these disciplines. Moreover, for problems concerning real flows, the imposition of exact boundary conditions on the equations of a CFD code is not always feasible as turbulence models are not always capable of encapsulating the inherent structure of the flow (Hayase, 2015).

As van Oudheusden *et al.* (2007) mention, the PIV measurement technique constitutes a non-intrusive method to study very complex flows and has emerged as an accurate and credible tool for fundamental and industrial fluid dynamics in-

vestigation over the last decades, being able to extract instantaneous velocity fields simultaneously over large domains of interest. Hence, the PIV technique is a natural selection for the purpose of combining measurements with CFD codes.

The fundamental idea has been introduced in the past. Hayase and Hayashi (1997) proposed a methodology where the SIMPLER algorithm uses partial experimental information as feedback for the reconstruction of the boundary conditions of turbulent simulations. Two other attempts may also be noted: Jaw *et al.* (2009) implemented a SIMPLER based method where 2D PIV data are integrated and the respective pressure fields of steady-state, incompressible, laminar flows are calculated, while Gunaydinoglu and Kurtulus (2020), again with a SIMPLER-based algorithm, extracted pressure fields of incompressible, laminar, steady as well as unsteady flows, utilising 2D PIV velocity data. Although the methodology of the two forenamed attempts is quite similar to the one presented here, they do not include turbulence closure. Regarding the computation of the pressure fields from PIV data, numerous endeavours based on the solution of a Poisson pressure equation can be found (Vanierschot and Van den Bulck, 2008, Suryadi and Obi, 2011, Van der Kindere *et al.*, 2019). It has to be noted though that in these methods PIV velocity fields remain unchanged and thus do not constitute measurement integration into CFD calculations per se.

The methodology that is implemented in the present endeavour is a SIMPLE algorithm-based one, where a finite volume method is applied for the discretisation of the 2D RANS equations, boundary conditions are imposed from unchanging PIV data and turbulence is included through the Reynolds Stresses, calculated directly from the statistics of the PIV experiment. The calculation procedure thus includes turbulence effects, avoiding the assumptions related to numerical turbulence closure models, and ensures conservation of mass and momentum through the solution of the corresponding equations. Furthermore, it arguably ensures better compliance of the CFD solution to the inherent physics of the flow being studied, since turbulence models are usually calibrated in order to be consistent with the prediction of fundamental flows e.g. homogeneous isotropic turbulence, logarithmic law boundary

layer etc. (Duraisamy *et al.*, 2019). The aforementioned methodology is applied for three regions lying on the symmetry plane of the flow around a cube with openings, immersed in a boundary-layer at an angle of attack equal to 0 degrees, utilising PIV data originating from the experiment of Manolesos *et al.* (2018).

## EQUATIONS AND ITERATIVE METHOD

In this section, the basic equations that are solved are presented. Firstly, the 2D steady-state Reynolds-Averaged Navier-Stokes (RANS) momentum equation (1) in tensor form is given along with the continuity equation (2), for incompressible flow. Although the continuity equation is not solved directly throughout this method, it is a key component as it is imperative for the deduction of the pressure correction equation (Patankar, 1980).

$$\rho \bar{u}_j \frac{\partial \bar{u}_i}{\partial x_j} = \frac{\partial \bar{p}}{\partial x_i} + \mu \Delta \bar{u}_i - \rho \left( \frac{\partial \overline{u'_i u'_j}}{\partial x_j} \right) \quad (1)$$

$$\frac{\partial \bar{u}_i}{\partial x_i} = 0 \quad (2)$$

Here  $i, j = 1$  or  $2$  (with respect to  $x$  and  $y$  direction),  $\Delta$  is the Laplace operator,  $\rho$  and  $\mu$  are the density and dynamic viscosity respectively and the last term on the right hand-side of the equation corresponds to the Reynolds Stress gradients.

By deploying the finite volume method in equation (1), a pentadiagonal linear system for each direction ( $x$  and  $y$ ) is derived, which is solved by the Alternating-Direction Implicit Method (ADI). Here, the terms corresponding to the Reynolds Stresses are included in the source terms of the discretised momentum equations, instead of being modelled. An analogous pentadiagonal linear system, corresponding to the pressure correction can be extracted (Patankar, 1980).

The Reynolds Stresses terms can be computed directly from the statistics of the experiment. If  $N$  is the total number of PIV snapshots then the equation, in tensor form, of these terms is written as follows:

$$\overline{u'_i u'_j} = \sum_{k=1}^N \frac{u'_{i,k} u'_{j,k}}{N} \quad (3)$$

The computational grid is almost identical to the PIV one, so interpolation is not necessary to produce the initial CFD values. The initial velocity field and of course the statistics for the Reynolds Stresses, for the commencement of the iterative algorithm, are provided by the PIV data.

This direct calculation of Reynolds Stresses from PIV data is evidently limited by the PIV resolved length/time scales, therefore a number of higher frequencies intrinsically linked to the nature of turbulent flows cannot be included. However, in the examined case, where the CFD grid is almost identical to the PIV one, the aforementioned physical limitation is assumed not to be crucial, since the CFD solution is not expected to resolve sub-PIV length/time scales.

The type of boundary conditions (BC) that is deployed imposes constant velocities and convective terms on a boundary zone which contains three lines/layers of grid points and two finite volumes adjacent to each boundary, respectively. Initial attempts to use Dirichlet boundary conditions at the

boundary nodes (i.e. constant velocities,  $u$  and  $v$  with respect to the  $x$  and  $y$  directions, and constant convective terms) were ineffective.

The modified SIMPLE iterative algorithm for the extraction of the results consists of the following steps:

1. The pressure correction equation is solved, after having introduced as initial velocity fields those emanating from the PIV measurements.
2. The adjusted/corrected velocity and pressure fields are calculated by implementing the standard SIMPLE correction equations.
3. The RANS momentum equations are solved with respect to the  $x$  and  $y$  direction with Reynolds Stresses included in the source terms of the discretised form of the equations.
4. The aforementioned iterative steps are repeated until there is the best possible convergence.

The method was developed using an in-house code, which is a standard finite volume implementation of the SIMPLE algorithm on a Cartesian grid with collocated variables and has been used in numerous studies e.g. Bouris and Bergeles (1999), Jurelionis and Bouris (2016) and Konstantinidis and Bouris (2016).

## RESULTS

### Configuration of the experiment

The configuration of the experiment that Manolesos *et al.* (2018) conducted at the National Technical University of Athens wind tunnel, in the large test section (2.5m×3.5m×12m) is given in Figure 1.

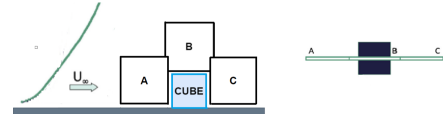


Figure 1. Geometry and configuration of the PIV experiment (Manolesos *et al.*, 2018). Left: side view with upstream velocity profile, Right: top view.

The present 2D method is applied to the case of high shear flow around the surface mounted cube immersed in a boundary-layer flow. The method has already been successfully applied to the case of a solid cube (Pallas and Bouris, 2022) but here, a more complex situation is considered where a thin vertical opening is present at the center of the upstream and downstream face of the cube (see Manolesos *et al.*, 2018). A, B and C are planes of symmetry and they are parallel to the vector of the free stream velocity. Owing to the assumed two-dimensional nature of the mean flow on these planes, results for plane A, B and C will be presented. Table 1 illustrates the basic grid and geometric parameters for the three planes. It is noted that the CFD spatial resolution is the same as the PIV one and that the PIV/CFD grid is uniform and collocated.

Apart from the PIV experiment, pressure taps, were utilised for the extraction of profiles of the pressure coefficient,  $C_{p,exp}$  (Manolesos *et al.*, 2017) along the plane of symmetry, on the centre line of the front, the roof and the back face walls of the cube (Figure 2), so they could be compared with the CFD-calculated  $C_p$  profiles. It should also be noted that the maximum experimental error of the pressure coefficient is equal to 4.5 %, (the maximum measurement errors of the pressure and the reference velocity are 3 % (Manolesos *et al.*, 2018) and 1.67 %, respectively).

It has to be clarified that the coordinates  $X, Y$  in all the forthcoming figures are non-dimensionalised with the height of the cube,  $H_c = 0.11$  m, whilst the thick black line represents the boundary of the cube. Moreover, the distance of

the three planes from every solid boundary (i.e. the ground and the respective walls of the cube) is close to 1cm (or 0.09 in non-dimensional form, so, e.g., for plane A, the point with  $X = X_{max}, Y = 0.91$  corresponds to the upper edge of the cube). The Reynolds number at cube height exceeded  $2 \cdot 10^4$  throughout the realisation of the experiment, namely it was over the suggested limit for Reynolds number independence in wind tunnel tests on buildings (Castro and Robins, 1977). It is noted that from now on, the overbar denoting time-averaged velocities will be omitted.

Plane	$NI$	$NJ$	$X_{tot}/H_c$	$Y_{tot}/H_c$
A	98	95	1.68	1.63
B	99	104	1.52	1.60
C	110	105	1.67	1.59

Table 1. Basic geometric and grid parameters:  $NI$  and  $NJ$  are the numbers of the grid lines with respect to the  $x$  and  $y$  direction, while  $X_{tot}$  and  $Y_{tot}$  are the  $x$  and  $y$  dimensions of the computational domain.

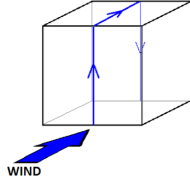


Figure 2. Pressure measurement locations (Manolesos *et al.*, 2017).

### Plane A

Figure 3a, presents the contours of the CFD total velocity  $U_{t,CFD}$ , extracted with the above-mentioned iterative methodology, whilst in Figure 3b those of the uncorrected PIV total velocity  $U_{t,PIV}$  are given, for the experiment on plane A.

As expected, the CFD-calculated velocity field is similar to the PIV one. More specifically, the position of the stagnation point, namely at approximately  $(X_{max}, 0.7)$ , and the velocity range remain almost invariant after the deployment of the CFD methodology. Figure 4a, where the relative error  $\varepsilon_{u_i}(\%) = 100 \cdot |u_{i,CFD} - u_{i,PIV}| / \langle u_{i,PIV} \rangle$  is presented ( $u_{i,CFD}$  and  $u_{i,PIV}$  are local, total, CFD and PIV velocities, respectively, whilst  $\langle u_{i,PIV} \rangle$  is the time and spatially averaged PIV total velocity), further supports the aforementioned argument. That is to say, its value is maximum only in the area near the top upstream corner of the cube where the flow accelerates, whereas in the rest of the domain the error remains below 10–20%. This possibly indicates that the CFD spatial resolution is inadequate to capture the physics of the flow near the cube's upstream corner.

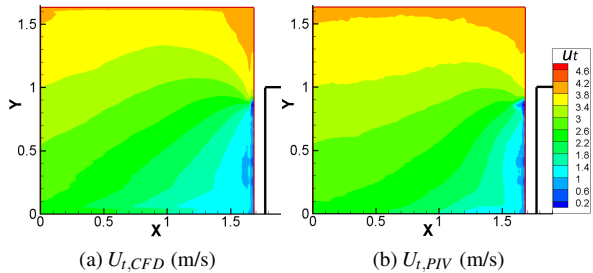


Figure 3. Contours of the total velocity extracted by: (a) CFD methodology, (b) PIV experimental technique, on plane A.  $X$  and  $Y$  are non-dimensional coordinates, whereas the thick black line denotes the upstream boundary of the cube. Flow is from left to right.

The normalised continuity residual,  $CRN$ , which is derived by implementing the discretised form of the continuity equation, using the PIV velocities on plane A before non-dimensionalising it with a characteristic velocity gradient i.e.  $\langle u_{t,PIV} \rangle / (2\Delta x)$ , is shown in the form of contours in Figure 4b. Similar to the error of Figure 4a,  $CRN$  reaches its highest values near the solid boundary of the cube, whereas its maximum appears near the top upstream corner. Owing to the strong coupling between the continuity residual and the SIMPLE pressure correction equation, one can contend that the appearance of the maximum relative error near the top upstream corner of the cube is partially justified by the fact that  $CRN$  also reaches its highest value there. The higher  $CRN$  values near the upstream wall of the cube could be attributed to three-dimensional structures of the flow, since the third velocity component,  $w$  is not included in the calculation of the continuity residual. More specifically, the ratio of the third, not included, velocity component,  $w$  (Manolesos *et al.*, 2018, performed Stereo-PIV), over the  $u$  velocity component reaches its maximum value, namely 60%, near the top upstream corner of the cube.

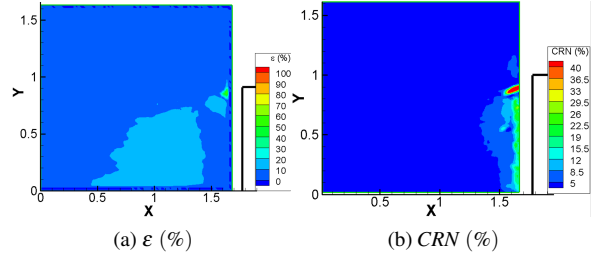


Figure 4. Contours of: (a) the non-dimensional error between the CFD total velocity,  $u_{t,CFD}$ , and the PIV one,  $u_{t,PIV}$ , on plane A, (b) the non-dimensional continuity residual derived by the discretised continuity equation,  $CRN$ , on plane A.  $X$  and  $Y$  are non-dimensional coordinates, whereas the thick black line denotes the upstream boundary of the cube. Flow is from left to right.

The pressure field of the experiment on plane A, with respect to a reference pressure located at the upstream boundary of the plane, chosen as the least disturbed point of the flow, is illustrated in Figure 5a. From the calculated pressure fields, the profile of the pressure coefficient  $C_p = (P - P_{ref}) / (1/2\rho U^2)$  (where  $P_{ref} = 0$  and  $P_{dyn} = 1/2\rho U^2 = 5.99\text{Pa}$ ) is extracted along the boundary that corresponds to the upstream face of the cube (at a distance of approximately 1 cm) and compared with the experimental  $C_{p,exp}$ , (Manolesos *et al.*, 2017) in Figure 5b.

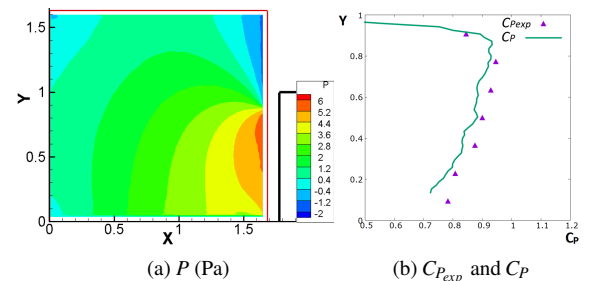


Figure 5. (a) Relative pressure contours extracted by the developed methodology, on plane A, (b) comparison between  $C_{p,exp}$  and  $C_p$ , where the  $Y$ -axis corresponds to the non-dimensional distance from the bottom boundary of the domain ( $Y = 0.91$  denotes the upper edge of the cube), for plane A. Flow is from left to right for (a).

The pressure contours, shown in Figure 5a, indicate the stagnation point (i.e.  $(X_{max}, 0.7)$ ), since the pressure reaches

its maximum value near this point, in line with the velocity behaviour shown in Figure 3. Near the corner, there is a pressure drop, due to flow acceleration.

Figure 5b, shows that there is a slight difference between the CFD-calculated pressure coefficient,  $C_P$ , and the experimental one,  $C_{P_{exp}}$ , i.e. the maximum difference is about 5 – 10% of  $C_{P_{exp}}$ , which is probably caused by: (i) the reference pressure is not exactly the same as the experimental reference one, which was outside the experimental domain available here, (ii) CP is calculated at a distance of approximately 1 cm and not exactly on the upstream wall, (iii) numerical and experimental errors, (iv) 3D effects (leading to increased PIV mass residual).

## Plane B

In Figure 6a, the contours of the CFD-calculated total velocity  $U_{t,CFD}$  are given, while in Figure 6b those of the PIV total velocity  $U_{t,PIV}$  are illustrated, for the experiment on plane B.

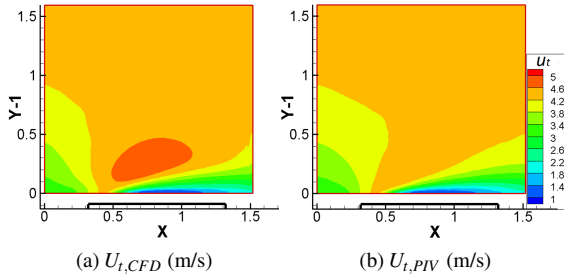


Figure 6. Contours of the total velocity extracted by: (a) CFD methodology, (b) PIV experimental technique, on plane B.  $X$  and  $Y$  are non-dimensional coordinates (non-dimensional distance of 1 corresponds to 1 cube height), whereas the thick black line denotes the roof of the cube. Flow is from left to right.

Similar to the case of plane A, the iterative method does not seem to change significantly the velocities on plane B. More specifically, the region of low velocities near the solid boundary of the cube remains almost invariant while the velocity range is almost the same for the CFD and PIV velocity fields. This indicates the potential of the proposed approach in terms of universality and independence of the specific characteristics of the flow velocities.

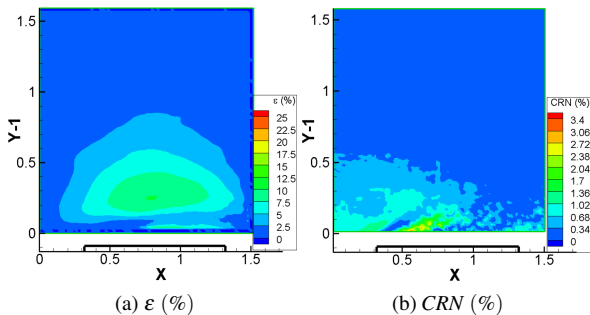


Figure 7. Contours of: (a) the non-dimensional error between the CFD total velocity,  $u_{t,CFD}$ , and the PIV one,  $u_{t,PIV}$ , for plane B, (b) the non-dimensional continuity residual derived by the discretised continuity equation,  $CRN$ , for plane B.  $X$  and  $Y$  are non-dimensional coordinates (non-dimensional distance of 1 corresponds to 1 cube height), whereas the thick black line denotes the roof of the cube. Flow is from left to right.

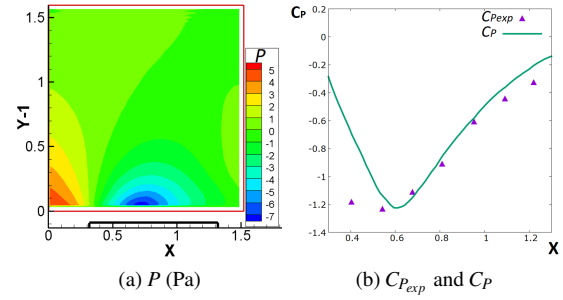


Figure 8. (a) Relative pressure contours extracted by the developed methodology, for plane B, (b) comparison between  $C_{P_{exp}}$  and  $C_P$ , where the  $X$ -axis corresponds to the non-dimensional distance from the upstream boundary of the domain, for plane B. Flow is from left to right for (a).

Figure 7a, where the error/difference between the initial PIV and the CFD-estimated velocities is shown, further supports that no significant corrections take place. More specifically, the maximum error is about 10% and appears in the area of flow acceleration. Generally, a comparison between the error of plane B and that of plane A, reveals that lesser correction takes place in plane B. This can be partially attributed to the much lower continuity residual, as its maximum value, shown in Figure 7b, is about ten times less than that in plane A. The ratio of the third, not included, velocity component,  $w$  (Manolesos *et al.*, 2018, performed Stereo-PIV), over the  $u$  velocity component (not shown) is close to zero in most parts of the examined domain except for the region near the roof of the cube where it is about 24%. This is generally better than in plane A and may partially justify the lower values of  $CRN$  for plane B in comparison with those for plane A.

The relative pressure field of the experiment on plane B, with respect to a reference pressure located at the top upstream corner of the domain (where the flow can be considered free stream) is illustrated in Figure 8a, whereas in Figure 8b a comparison between  $C_P$  and  $C_{P_{exp}}$  (Manolesos *et al.*, 2017) is presented for plane B. It should be noted that the reference pressures in planes A, B (and C, presented following) could be significantly different.

Figure 8a presents a physically consistent behaviour of pressure. That is to say, it reaches its maximum value near the inlet, namely 5 Pa above the free stream value, as it is influenced by the stagnation that takes place on the upstream solid boundary of the cube. After the region of positive pressures, there is a pressure drop due to flow acceleration, a conclusion in line with the results of other researchers, such as Hölischer and Niemann (1998), Castro and Robins (1977).

Regarding the comparison between  $C_{P_{exp}}$  and  $C_P$ , it can be said that the calculated pressure coefficient is close to the measured values with an exception being the first measurement point where a large difference can be observed. This probably indicates that the spatial resolution in conjunction with Neumann boundary conditions, are incapable of depicting suitably the local physics of the flow, i.e. the steep pressure gradient. The fact that velocity measurements could not be performed up to the surface where pressure was measured exacerbates this. Indicative remedies for this drawback of the developed approach will be given in the section of conclusions.

## Plane C

Figure 9 illustrates the contours of the CFD-calculated total velocity  $U_{t,CFD}$  as well as those of the PIV total velocity  $U_{t,PIV}$ , for plane C.

A characteristic element of the experiment on this domain, is the flow out of the opening on the downstream face of the cube (at  $X = 0$  and  $Y = 0$  to 1).

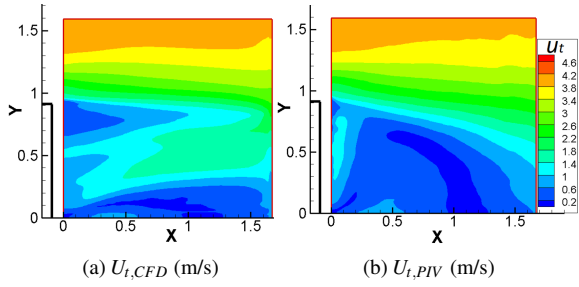


Figure 9. Contours of the total velocity extracted by: (a) CFD methodology, (b) PIV experimental technique, on plane C.  $X$  and  $Y$  are non-dimensional coordinates, whereas the thick black line denotes the downstream boundary of the cube. Flow is from left to right.

Although the velocity range remains invariant after the iterative method, significant modifications are observed in the region of low total velocities in the wake of the cube. Figure 10a supports the forenamed statement, since the normalised error/difference between the PIV and CFD velocities reaches a maximum value of 90 %. More specifically, there is an extended area coinciding with that of almost zero total velocities, where the error is higher than 50%.

The fact that the continuity residual shown in Figure 10b reaches a maximum value of 23%, namely a value of  $CRN$  lower than that for plane A, probably indicates that the mass residual of the domain does not constitute the most critical parameter for the departure of the CFD velocity field from that of the PIV measurements. It has to be noted that the highest  $CRN$  values are observed near the solid boundary of the cube, which is in line with the results for plane A.

The ratio of the third velocity component,  $w$ , (Manoleos *et al.*, 2018, performed Stereo-PIV), over the  $u$  velocity component (not shown here) generally is higher than that of the above-presented planes. However, the highest values are observed at points where the  $u$  velocity component is close to zero. Moreover, if three-dimensional flow structures were predominant, this would also be manifested in an increase of the values of  $CRN$ , whose values however, in this case, remain moderate.

All the aforementioned analysis, indicates that one might seek the reason for this discrepancy between the CFD and PIV velocities in the low CFD spatial resolution, since it is probably inadequate to capture the complex physics of the flow behind a bluff body such as the cube.

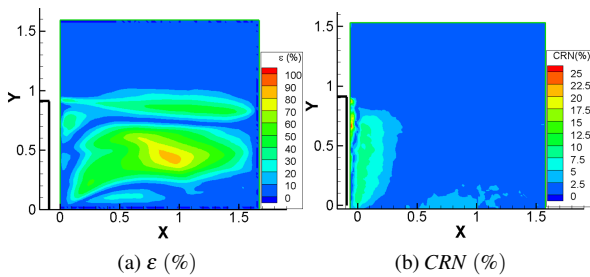


Figure 10. Contours of: (a) the non-dimensional error between the CFD total velocity,  $u_{t,CFD}$ , and the PIV one,  $u_{t,PIV}$ , on plane C, (b) the non-dimensional continuity residual derived by the discretised continuity equation,  $CRN$ , on plane C.  $X$  and  $Y$  are non-dimensional coordinates, whereas the thick black line denotes the downstream boundary of the cube. Flow is from left to right.

The relative pressure field of the measurements on plane C, with respect to a reference pressure located at the top downstream corner of the domain, again different from planes A and B but chosen as the point where the flow is the least disturbed, is illustrated in Figure 11a, whereas in Figure 11b a comparison between  $C_P$  and  $C_{P_{exp}}$  is presented.

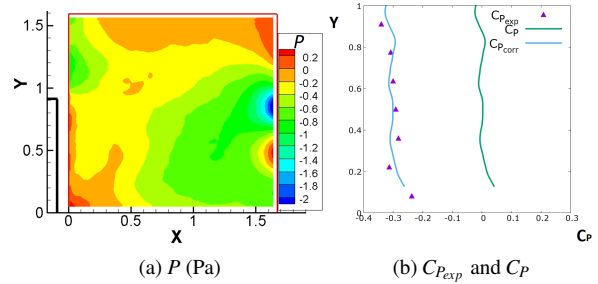


Figure 11. (a) Relative pressure contours extracted by the developed methodology, on plane C, (b) comparison between  $C_{P_{exp}}$  and  $C_P$ , where the  $Y$ -axis corresponds to the non-dimensional distance from the bottom boundary of the domain ( $Y = 0.91$  denotes the upper edge of the cube), for plane C. Flow is from left to right for (a).

In Figure 11a, a relatively small range of pressure can be observed, namely about 2 Pa, indicating that the pressure is generally constant in the wake of the cube, as expected, due to flow separation. Two lobe-like structures with a pressure difference equal to the pressure range, are located close to each other on the downstream boundary of the domain, which are probably caused by the inadequacy of the Neumann boundary conditions that are imposed on this area.

Unlike the results shown for plane A and B, the comparison between  $C_{P_{exp}}$  (purple points) and  $C_P$  (green line) reveals a significant discrepancy between computational results and measurements. It has to be clarified that the most probable reasons are: (i) the reference pressure is not exactly the same as the experimental reference one, which was outside the experimental domain available here, (ii)  $C_P$  is calculated at a distance of approximately 1 cm and not exactly on the downstream wall (iii) numerical and experimental errors and (iv) 3D effects.

The mean value of the difference  $\Delta C_P = C_{P_{exp}} - C_P$  for every measurement point, is found to be equal to  $\overline{\Delta C_P} = -0.3043$  while its standard deviation in  $C_P$  units is equal to 0.0197, results that correspond to 1.8 Pa and 0.12 Pa respectively (the dynamic pressure is once again equal to 5.99 Pa). Based on the aforementioned results, it can be contended that the discrepancy between the two  $C_P$  profiles has similar properties to a systematic error/bias, most probably corresponding to a difference between the experimental and computational reference pressures.

The blue line, shown in Figure 11b, is produced by adding  $\Delta C_P = -0.3043$  to the CFD-calculated pressure coefficient. The measurements almost coincide with the corrected pressure coefficient, with the maximum value of the relative error,  $\Delta C_P / C_{P_{exp}}$ , derived about 7 %.

Generally, the results regarding plane C for the examined case where the apertures are open, demonstrate a larger, probably aberrant, velocity correction as well as a higher discrepancy between the experimental and CFD  $C_P$  profiles, in comparison with the results extracted for the case where the apertures are closed (Pallas and Bouris, 2022).

## CONCLUSIONS

Two-dimensional time-averaged PIV velocity fields along with PIV statistics have been integrated in a code based on the

SIMPLE algorithm, and attempt is made to apply the methodology to three different data sets lying on the upstream, downstream and roof plane of symmetry, respectively, for the case of turbulent flow around a surface-mounted cube, with upstream and downstream face vertical openings. The extraction of the respective pressure fields as well as the correction of the PIV velocity fields in order to satisfy the continuity equation are undertaken, whereas no model of turbulence is necessary, since the closure of the equations is accomplished by direct computation of the Reynolds Stresses, using the PIV statistics.

Profiles of the pressure coefficient near the upstream, roof and downstream solid boundaries, calculated by the CFD method, are compared with experimentally derived  $C_p$  profiles, revealing that in most cases, the proposed approach is capable of producing reliable and physically consistent results.

Although the implementation of the approach to a more complex case than in Pallas and Bouris (2022) and in three regions of the flow with different inherent physics does prove to a certain extent its flexibility and universality, several major issues remain, such as the availability of the experimental data, the PIV temporal and spatial resolution as well as the CFD spatial resolution, the uncertainties in the data and finally, the two-dimensionality assumption of the flow.

A prerequisite for the application of the developed approach, is the existence of PIV measurement data, which is not always feasible, but even when a PIV experiment can be carried out, optical access problems (predominant for cases of complex geometry) as well as limitations linked to the resolved PIV length/time scales can deteriorate the quality of the results. The PIV-resolved length/time scales (and the respective frequencies) do not constitute an important limiting factor, whenever the spatial PIV and CFD resolution are similar, since the CFD solution is not expected to resolve sub-PIV length/time scales.

As seen in the presented results and especially for plane C, the spatial PIV/CFD resolution is not always adequate to capture complex physics of the flow in regions of steep gradients, e.g., the upstream corner or the wake of the cube. This problem may be attenuated by applying interpolation of the PIV data to a finer grid and/or by implementing CFD local grid refinement techniques.

Finally, it should be noted that the violation of the assumption of two-dimensionality of the flow, can degrade the quality of the extracted results. The SIMPLE algorithm is based on the solution of a pressure correction equation which is strongly coupled with the continuity/mass residual through its source terms. Owing to the non-inclusion of the third velocity component,  $w$ , it can be contended that the appearance of three-dimensional flow structures can jeopardise the credibility of the the proposed approach, since they could lead to increased values of the initial PIV continuity residual.

To conclude, the proposed method, in most cases, yielded reliable and physically consistent results, showing the potential of performing adequately for different conditions and different intrinsic flow physics. Although several issues remain, this attempt shows promise as a complementary source of information for experimental measurements, as a source of correction for numerical simulations and/or as a possible benchmark for numerical model development. More specifically, the fact that PIV-calculated Reynolds stresses are introduced in the source terms of the RANS equations, overcomes any assumptions inherent in a turbulence model, and possibly leads to better compliance of the CFD solution to the inherent physics of the flow, since turbulence models are usually calibrated in order to be consistent in the prediction of fundamental flows

(Duraisamy *et al.*, 2019).

## REFERENCES

- Bouris, D. & Bergeles, G. 1999 Two dimensional time dependent simulation of the subcritical flow in a staggered tube bundle using a subgrid scale model. *International journal of heat and fluid flow* **20** (2), 105–114.
- Castro, I. P. & Robins, A. G. 1977 The flow around a surface-mounted cube in uniform and turbulent streams. *Journal of fluid Mechanics* **79** (2), 307–335.
- Duraisamy, K., Iaccarino, G. & Xiao, H. 2019 Turbulence modeling in the age of data. *Annual Review of Fluid Mechanics* **51**, 357–377.
- Gunaydinoglu, E. & Kurtulus, D. F. 2020 Pressure–velocity coupling algorithm-based pressure reconstruction from piv for laminar flows. *Experiments in Fluids* **61** (1), 1–20.
- Hayase, T. 2015 A review of measurement-integrated simulation of complex real flows. *Journal of Flow Control, Measurement & Visualization* **3** (02), 51.
- Hayase, T. & Hayashi, S. 1997 State estimator of flow as an integrated computational method with the feedback of online experimental measurement. *Journal of Fluids Engineering, Transactions of the ASME* **119** (4), 814–822.
- Hölscher, N. & Niemann, H. J. 1998 Towards quality assurance for wind tunnel tests: A comparative testing program of the windtechnologische gesellschaft. *Journal of Wind Engineering and Industrial Aerodynamics* **74**, 599–608.
- Jaw, S. Y., Chen, J. H. & Wu, P. C. 2009 Measurement of pressure distribution from piv experiments. *Journal of Visualization* **12** (1), 27–35.
- Jurelionis, A. & Bouris, D. 2016 Impact of urban morphology on infiltration-induced building energy consumption. *Energies* **9** (3), 177.
- Van der Kindere, J. W., Laskari, A., Ganapathisubramani, B. & De Kat, R. 2019 Pressure from 2d snapshot piv. *Experiments in fluids* **60** (2), 32.
- Konstantinidis, E. & Bouris, D. 2016 Vortex synchronization in the cylinder wake due to harmonic and non-harmonic perturbations. *Journal of Fluid Mechanics* **804**, 248–277.
- Manolesos, M., Gao, Z. & Bouris, D. 2018 Experimental investigation of the atmospheric boundary layer flow past a building model with openings. *Building and Environment* **141**, 166–181.
- Manolesos, M., Gao, Z., Xing, Z., Panos, M. & Bouris, D. 2017 Experimental study of the flow past a cube with openings embedded in a turbulent boundary layer. In *10th International Symposium on Turbulence and Shear Flow Phenomena*.
- van Oudheusden, B. W., Scarano, F., Roosenboom, E. W. M., Casimiri, E. W. F. & Souverein, L. J. 2007 Evaluation of integral forces and pressure fields from planar velocimetry data for incompressible and compressible flows. *Experiments in fluids* **43** (2), 153–162.
- Pallas, N. P. & Bouris, D. 2022 Calculation of the pressure field for turbulent flow around a surface-mounted cube using the simple algorithm and piv data. *Fluids* **7** (4), 140.
- Patankar, S. V. 1980 *Numerical heat transfer and fluid flow* (1st ed.). CRC press.
- Suryadi, A. & Obi, S. 2011 The estimation of pressure on the surface of a flapping rigid plate by stereo piv. *Experiments in fluids* **51** (5), 1403–1416.
- Vanierschot, M. & Van den Bulck, E. 2008 Planar pressure field determination in the initial merging zone of an annular swirling jet based on stereo-piv measurements. *Sensors* **8** (12), 7596–7608.